Materials Science Forum Vols. 633-634 (2010) pp 353-363

doi:10.4028/www.scientific.net/MSF.633-634.353

Microstructure Development and Ductility of Ultra-Fine Grained Mg-Gd Alloy Prepared by High Pressure Torsion

Jakub Cizek[1, a], Ivan Prochazka[1], Bohumil Smola[1], Ivana Stulikova[1], Vladivoj Očenášek[2], Rinat K. Islamgaliev[3] and Olya Kulyasova[3]

[1]Faculty of Mathematics and Physics, Charles University, Prague, Czech Republic

[2]Research Institute of Metals, Panenske Brezany 50, CZ-25070 Odolena Voda, Czech Republic

[3]Institute of Physics of Advanced Materials, Ufa State Aviation Technical University, Ufa 450000, Russia.

[a]jakub.cizek@mff.cuni.cz

Keywords: Mg-alloys, positron annihilation, high pressure torsion, ductility.

Abstract. Microstructure of ultra fine grained (UFG) Mg-Gd alloy prepared by high-pressure torsion (HPT) was investigated in the present work. Lattice defects introduced by HPT were characterized at first. Subsequently thermal stability of UFG structure and its development with annealing temperature were studied and correlated with changes of hardness and ductility. Precipitation effects in the alloy with UFG structure were compared with those in a conventional coarse-grained alloy. Defect studies were performed by positron annihilation spectroscopy (PAS), which represents well established non-destructive technique with a high sensitivity to open volume lattice defects like vacancies, dislocations, misfit defects etc. PAS investigations were combined with transmission electron microscopy (TEM) and X-ray diffraction (XRD). Changes of mechanical properties were monitored by Vicker's microhardness (HV) and deformation tensile tests. It was found that HPT deformed Mg-Gd alloy exhibits UFG structure with mean grain size of 100 nm and a dense network of dislocations distributed uniformly throughout the whole sample. Although recovery of dislocations takes place at relatively low temperatures, it is not accompanied by grain growth and the mean grain size remains around 100 nm up to 300°C. Tensile tests performed at elevated temperatures to examine ductility showed that HPT-deformed alloy exhibits a superplastic behavior at 400°C. Moreover, it was found that the precipitation sequence in HPT-deformed alloy differs from that in conventional coarse-grained material.

Introduction

Low density Mg-based alloys allow for a significant weight reduction which raises the effectiveness in a broad range of industrial applications, especially in automotive and aeronautical industry. Unfortunately, applicability of majority of classical Mg alloys is restricted to low temperatures due to a degradation of their mechanical properties above 200°C. There are several approaches how to overcome this problem. Particularly promising way is use of non-traditional rare-earth alloying elements [1]. Mg-Gd system is one example of such promising novel alloy. At elevated temperatures Gd exhibits relatively good solubility in Mg (up to 23.5 wt.%) but it rapidly decreases with decreasing temperature [2]. This makes possible to achieve sufficient hardness by formation of fine metastable precipitates of Gd-rich phases. It was found that supersaturated solid solution (sss) of Mg-Gd system undergoes with increasing temperature the following decomposition sequence [3,4]:

$$\text{sss} \rightarrow \beta'' \text{ (D019)} \rightarrow \beta' \text{ (c-bco)} \rightarrow \beta \text{ (cubic, } Mg_5Gd \text{ stable)}. \quad (1)$$

The β'' metastable phase is fully coherent with Mg matrix. This coherence is lost at some interfaces when phase transition into metastable β' phase with c-bco structure takes place. Plate shape particles of β' have the following orientation relationship with the Mg lattice: $[0001]_{Mg} \,||\, [001]_{c\text{-}}$

$_{bco}$ and $\{2\bar{1}\bar{1}0\}_{Mg} \,||\, (100)_{c\text{-}bco}$ [3]. Fine plates of β' phase precipitate in all the three possible orientation relationship modes cause remarkable hardening [3]. The stable β phase precipitates formed at higher temperatures are completely incoherent with Mg matrix.

Despite favorable strength and thermal stability, a disadvantage of Mg-Gd alloys consists in a poor ductility insufficient for most of potential industrial applications. Grain refinement is a well-known method how to improve ductility of metallic materials. Hence, severe plastic deformation, which is able to fabricate UFG structure, could represent a promising way for improvement of ductility of non-traditional Mg-alloys with rare-earths elements due to the effects of an extreme grain size reduction.

The aim of this work is microstructure characterization of binary Mg-Gd alloy prepared by HPT [5] and its comparison with microstructure of corresponding coarse-grained material. Subsequently, decomposition of supersaturated solid solution and precipitation effect in HPT-deformed and coarse-grained alloy were compared. Ductility of HPT-deformed alloy was studied using deformation tensile tests and was compared with ductility of the coarse-grained alloy. Hardening effects were monitored by HV testing.

Defects introduced by severe plastic deformation play key role in unique properties of UFG structure. Detailed characterization of these defects represents, therefore, an important task in microstructure investigations of the UFG materials. For this reason we employed PAS, a well established non-destructive technique with a high sensitivity to open-volume defects like vacancies, dislocations, etc. [6]. Positron lifetime (LT) spectroscopy, which enables to identify defects and to determine defect concentrations in studied specimens, was used as a principle experimental tool in this work.

Experimental

Mg-9.33wt.%Gd (Mg9Gd) alloy was prepared by squeeze casting. Results of chemical analysis of this alloy are given in Table 1. The as-cast alloy was subjected to a solution annealing at 500°C for 6 hours. This treatment is sufficient to dissolve Gd completely in Mg matrix [3]. The solution annealing was finished by quenching into water of room temperature. To create the UFG structure, the solution treated Mg9Gd alloy was deformed by HPT at room temperature using 5 rotations under a high pressure of 6 GPa. Details about the HPT procedure can be found in Ref. [5]. The HPT-treated specimens are disk shaped with a diameter of ≈ 12mm and a thickness of ≈ 0.3 mm.

Table 1 Chemical composition (in weight %) of the studied Mg9Gd alloy.

Specimen	Gd	Mn	Fe	Zn	Al	Si	Cu	Ni	Mg
Mg9Gd	9.33	0.014	0.020	0.0001	0.0077	0.0090	0.0026	0.0004	balance

After detailed characterization of as-deformed microstructure, the specimens were subjected to step-by-step (20°C /20 min) isochronal annealing to investigate development of microstructure with temperature and precipitation effects. Each annealing step was finished by quenching into water at room temperature.

A fast-fast LT spectrometer similar to that described in [7] with time resolution of 160 ps (FWHM ^{22}Na) was used in this work. TEM observations were carried out on a JEOL 2000 FX electron microscope operating at 200 kV. Optical microscopy (OM) was performed at metallographic microscope Arsenal AM-2T. HV was measured at a load of 100 g applied for 10 s using a STRUERS Duramin 2 hardness tester. Deformation tensile tests with a constant strain rate were performed at a tensile testing machine designed specifically for testing of small specimens [8].

Results and Discussion

Solution treated alloy. Fig. 1A shows an OM image of solution treated Mg9Gd alloy. A representative TEM image of this specimen is shown in Fig. 1B. The solution treated Mg9Gd specimen exhibits coarse grains with mean grain size ~ 200 μm and low density of dislocations.

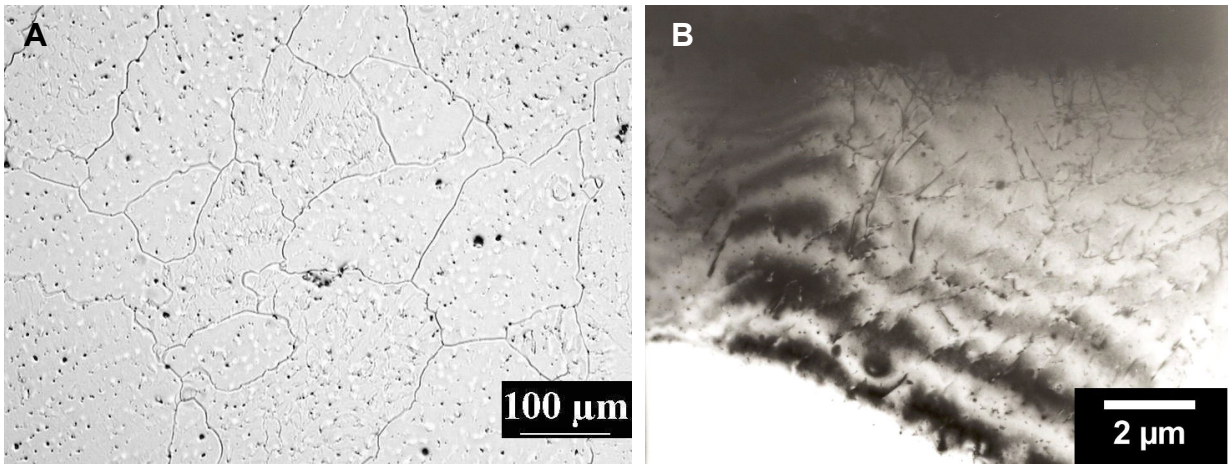

Fig. 1 Solution treated Mg9Gd alloy: (A) OM metallographic image of chemically etched specimen, (B) a representative TEM image.

Lifetimes and relative intensities of the components resolved in LT spectra are listed in Table 2. Results for a reference pure Mg (99.999%) specimen well-annealed at 280°C for 30 min are shown in the first line in the table. The reference pure Mg specimen exhibits a single-component spectrum with lifetime τ_B = (225.3 ± 0.4) ps, which is in a reasonable agreement with the lifetime of free, delocalized positrons in perfect Mg crystal determined by first principle calculations [4]. Hence, defect density in the reference Mg specimen is very low and virtually all positrons annihilate from the free, delocalized state.

Table 2 A summary of LT spectroscopy and HV measurements.

Sample	τ_1 (ps)	I_1 (%)	τ_2 (ps)	I_2 (%)	τ_f (ps)	HV (MPa)
Mg (99.999%), well annealed	225.3 ± 0.4	100	-	-	-	440 ± 40
Mg9Gd, solution treated	220± 4	90.9 ± 0.6	301 ± 2	9.1 ± 0.7	226 ± 1	680 ± 30
Mg9Gd, HPT-deformed (center)	180 ± 4	34 ± 2	256 ± 3	66 ± 2	224 ± 1	1670 ± 40
Mg9Gd, HPT-deformed (edge)	130 ± 9	12 ± 1	256 ± 2	88 ± 2	229 ± 2	2330 ± 40

If some specimen contains defects, which trap positrons, then (i) a new component (with lifetime $\tau_2 > \tau_B$) coming from positrons localized at defects appears in LT spectrum, and (ii) lifetime τ_1 of the shorter component becomes shortened ($\tau_1 < \tau_B$). It can be shown that in the frame of two-state simple trapping model (STM) [9] the quantity τ_f calculated as

$$\tau_f = \left(\frac{I_1}{\tau_1} + \frac{I_2}{\tau_2} \right)^{-1} \qquad (2)$$

equals to the lifetime of free positrons in a perfect (defect-free) material, i.e.

$$\tau_f \equiv \tau_B \,. \tag{3}$$

The relation (3) is often used to check consistency of decomposition with the two-state STM, i.e. whether the assumptions of STM (single type of defects, no de-trapping, uniform distribution of defects etc.) are fulfilled. The quantities τ_f calculated for various specimens using Eq. (2) are included in Table 2.

The solution treated Mg9Gd specimen exhibits two component LT spectrum. The dominant shorter component with lifetime τ_1 and intensity I_1 comes from free positrons not localized at defects. On the other hand, a weak longer component with lifetime τ_2 represents a contribution of positrons trapped at defects. One can see in Table 2 that relation (3) is satisfied for this decomposition testifying that solution treated alloy contains just a single type of defects. The lifetime $\tau_2 \approx 300$ ps agrees well with the calculated lifetime of positrons trapped at Mg-vacancies [4]. However, it is well known that vacancies in Mg become mobile well below room temperature [10]. As a consequence, thermal vacancies quickly disappear in a specimen quenched to room temperature. Hence, the vacancies detected in the solution treated Mg9Gd specimen must be stabilized by Gd atoms. Indeed, presence of Gd atoms attached to quenched-in vacancies was proved by coincidence Doppler broadening spectroscopy [4].

HPT-deformed alloy. A bright-field TEM image and an electron diffraction pattern for the HPT-deformed Mg9Gd alloy are shown in Fig. 2.The image shows a uniform UFG microstructure with a mean grain size of about 100 nm and a high density of dislocations distributed uniformly throughout the whole specimen. The electron diffraction pattern shows high-angle missorientation of neighboring grains.

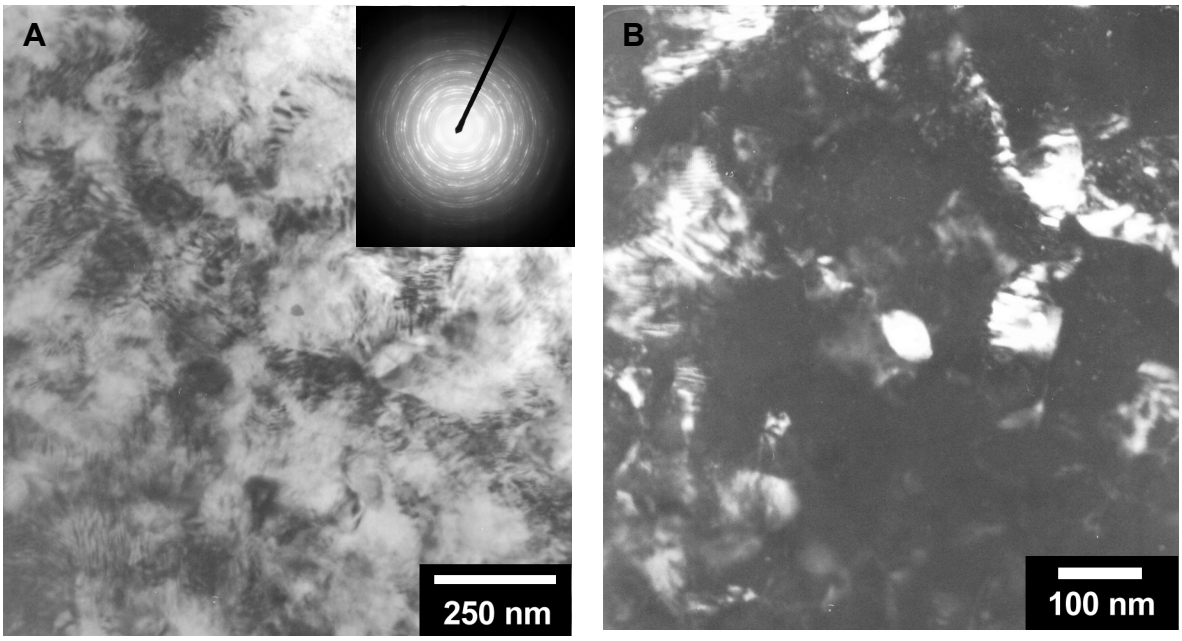

Fig. 2 HPT-deformed Mg9Gd alloy: (A) a representative bright-field TEM image and electron diffraction pattern, (B) a dark-field TEM image.

The LT spectrum of the HPT-deformed Mg9Gd alloy consists of two components, see Table 2. The first component with a lifetime $\tau_1 < \tau_B$ arises from the free positrons, while the second component represents a contribution of positrons trapped at defects. The lifetime τ_2 of the second component corresponds well with the lifetime of positrons trapped at Mg-dislocations [11]. One can see in Table 2 that the quantity τ_f calculated from Eq. (2) agrees well with τ_B, i.e. the relation (3) is

satisfied for HPT-deformed Mg9Gd alloy. This finding testifies uniform spatial distribution of dislocations in HPT-deformed Mg9Gd alloy.

Detailed mapping of the spatial distribution of dislocations on macroscopic scale was performed by extended HV measurements at various positions on the HPT-deformed specimen. These measurements confirmed axial symmetry of dislocation density with respect to the symmetry axis of the specimen disk. Dependence of HV on the radial distance r from the center of the HPT-deformed Mg9Gd sample disc is plotted in Fig. 3. One can see in the figure that HV increases from the center of the disc towards the margin of the specimen reflecting an increase of dislocation density with r. Relative difference in microhardness between the center and the edge is $\Delta HV/HV \sim 40$ %. This difference is however, substantially smaller than the relative increase of microhardness caused by HPT deformation (i.e. relative difference in HV between HPT-deformed and solution treated alloy) which approaches 200%. Enhanced dislocation density at the edge of the HPT-deformed Mg9Gd specimen was confirmed also by LT spectroscopy. Results of LT measurements performed at the center of the HPT-deformed specimen ($r = 0$ mm) and close to the edge of the specimen ($r = 4$ mm) are compared in Table 2.

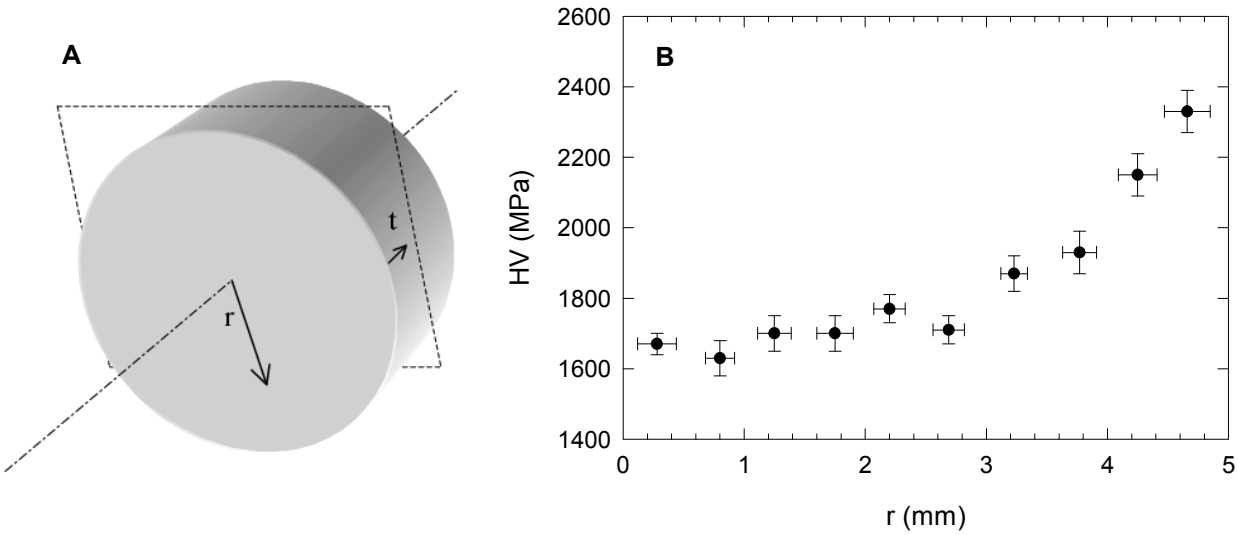

Fig. 3 (A) A schematic picture of HPT-deformed disc shaped specimen, (B) dependence of HV on the radial distance r from the center of the specimen. Each point in the figure is an average of 10 measurements performed at the same radial distance r from the center.

Thermal stability of microstructure. After characterization of the solution treated and HPT-deformed microstructure, the specimens were subjected to isochronal annealing in order to investigate the development of microstructure with increasing temperature and the recovery of defects.

Temperature dependence of HV on the annealing temperature for the solution treated Mg9Gd alloy is plotted in Fig. 4A. The LT spectra of the solution treated alloy are well fitted by two components at all annealing temperatures. At some temperatures the longer component corresponding to positrons trapped at defects even disappeared and the sample exhibited only a single component LT spectrum. Figs. 4B shows dependence of the intensity I_2 of positrons trapped at defects on the annealing temperature. The development of microstructure and precipitation effects in the solution treated Mg9Gd alloy were discussed in details in Ref. [4]. Therefore, here we mention only a few features important for comparison of the solution treated alloy with the HPT-deformed specimen. As one can see in Fig. 4B quenched-in vacancies are annealed out already at 80°C, which is reflected by a drop of I_2. Formation of β'' phase particles coherent with Mg matrix

occurs from 100°C. Fine coherent β'' particles have a remarkable hardening effect and cause also a rise in I_2, see Figs. 4A and 4B. This indicates that β'' particles contain vacancies, which trap positrons. One can assume that Gd-rich clusters are formed at the early stages of precipitation of β'' phase. Long-range diffusion of Gd atoms is vacancy-assisted and the Gd-rich clusters or small particles are associated with vacancy-like defects, which represent trapping sites for positrons. A similar effect, i.e. the formation of small Sn clusters associated with vacancy like defects, was observed recently in an Al–Sn alloy [12].

Further annealing at temperatures above 160 °C leads to a partial dissolution of the β'' phase particles and to precipitation of semicoherent (c-bco) β' phase. Open-volume misfit defects are present at the β' phase particle interface where the coherence with the matrix is lost. The misfit defects provide trapping sites for positrons with an open volume comparable to that of vacancy. As a consequence the β' phase precipitation causes an increase in I_2, see Fig. 4B. Particles of stable β phase are formed by annealing at temperatures higher than 300°C. The β phase particles are incoherent with Mg matrix. Therefore, one can expect that misfit defects are present at the β phase precipitate-matrix interfaces. However, TEM studies of Mg–15wt%Gd solution treated alloy revealed that the β phase precipitates as large plates lying parallel to the $\{10\bar{1}0\}$ planes of the Mg matrix. It is energetically favorable because the misfit in this plane is small. Thus, open-volume misfit defects capable of positron trapping are expected only to be present at the edges of the plate shaped β phase precipitates. Significantly larger sized β phase precipitates result in a substantially lower fractional area of the edges compared to the fine β' phase precipitates. The distance between the coarse β phase particles also becomes larger. Moreover, the volume fraction of the β phase precipitates is lower because the higher temperature leads to increased solubility of Gd in Mg matrix. All these factors result in a lower volume fraction of the misfit defects and thereby to a reduced positron trapping compared to the β' phase precipitates. Indeed, no changes in I_2, which could be interpreted by the formation of β phase particles, took place in the solution treated Mg9Gd alloy studied in the present work. This indicates that the concentration of the misfit defects is too low to be detected by PAS.

The solid solution of Gd in Mg is restored in Mg9Gd specimen by annealing above 460°C. Analogically to the solution treatment thermal vacancies become associated with diluted Gd atoms and vacancy–Gd pairs are formed. The thermal vacancies not associated with Gd atoms disappeared quickly after quenching the annealed specimen to room temperature. Thus, only those vacancies bound to Gd atoms remain in the specimen quenched to room temperature.

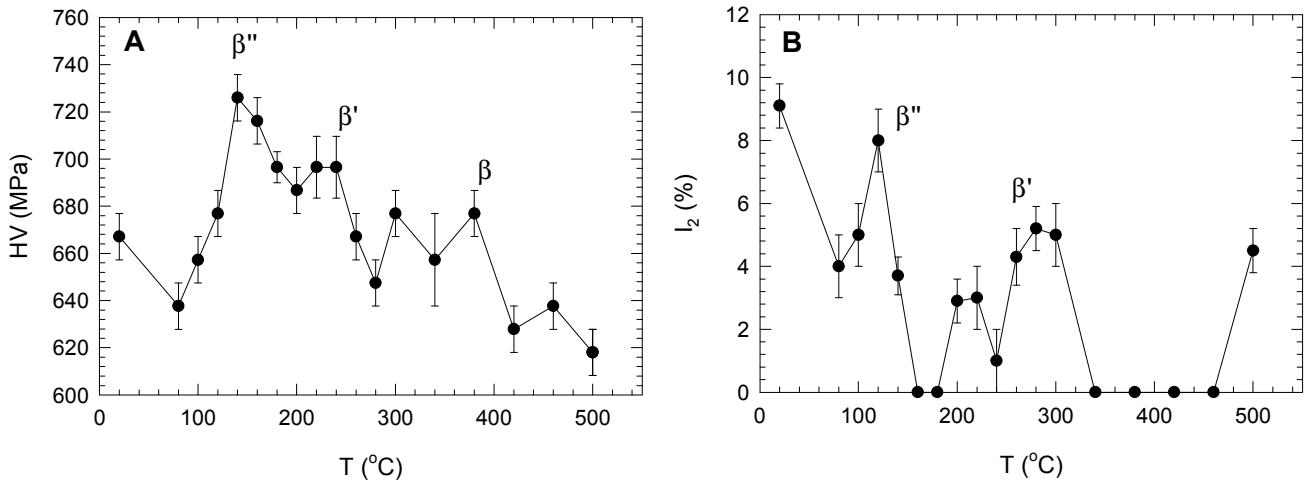

Fig. 4 Solution treated Mg9Gd alloy: (A) temperature dependence of HV, (B) temperature dependence of intensity I_2 of positrons trapped at defects.

Temperature dependence of HV measured on HPT-deformed Mg9Gd is plotted in Fig. 5A. As HV increases from the center of the specimen towards margin, Fig. 5A shows minimum HV value measured at the center and also maximum HV value measured at the edge. The LT spectra of HPT-deformed Mg9Gd alloy are well fitted by two components. The lifetime τ_2 did not change with annealing temperature (except for some statistical fluctuations) indicating that the nature of positron traps remains unchanged. The intensity I_2, which represents a contribution of positrons trapped at defects, is plotted in Fig. 5B as a function of annealing temperature.

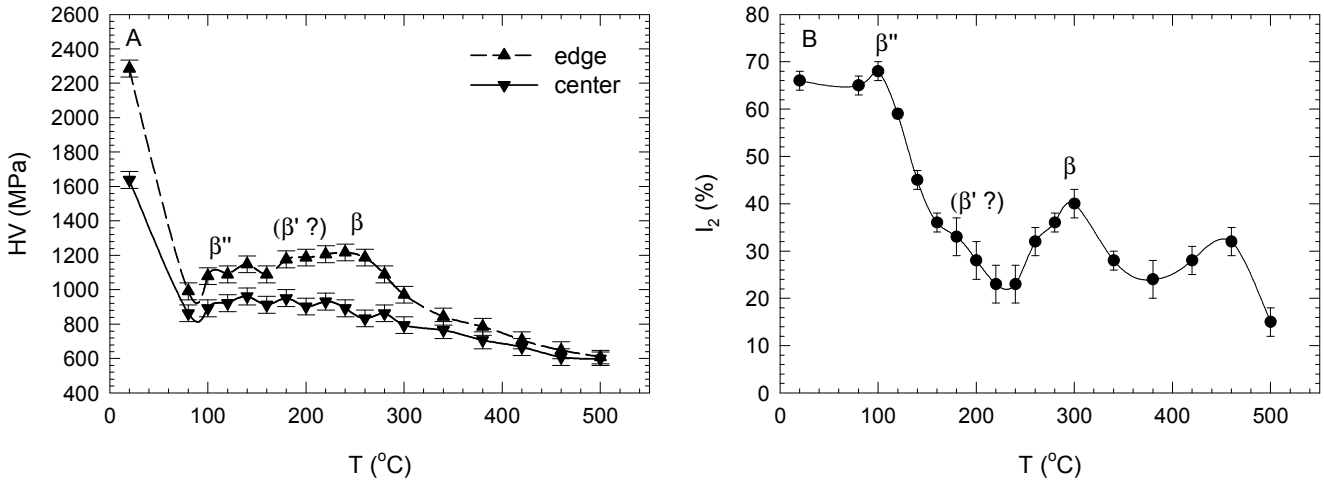

Fig. 5 HPT-deformed Mg9Gd alloy: (A) temperature dependence of HV measured at the center of the sample (r = 0 mm, downward triangles) and at the edge (r = 5 mm, upward triangles), (B) temperature dependence of intensity I_2 of positrons trapped at defects.

Two effects can be observed in HPT-deformed Mg9Gd alloy with increasing temperature: (i) recovery of defects introduced by severe plastic deformation, and (ii) precipitation effects due to decomposition of supersaturated solid solution. One can see in Fig. 5B that I_2 drastically decreases in the temperature interval (100–220°C) testifying a significant recovery of dislocations in this temperature range. A slight local increase in I_2 at 100°C, i.e. prior to the main drop due to recovery of dislocations, is most probably caused by formation of the β'' phase as confirmed by coincidence Doppler broadening [13]. However, the β'' phase particles are very fine (10 nm in diameter or less) and were thus not observed by TEM. It should be noted, that the high dislocation density makes TEM observation of fine precipitates very difficult. It can be seen in Fig. 5A that HV falls abruptly after anneal at 80°C, i.e. it precedes the strong decrease in I_2, see Fig. 5B. It indicates that there is a remarkable softening, which seems to occur prior to the decrease in dislocation density. It could be connected with some rearrangement of dislocations without significant change of the net dislocation density or by relaxation of internal stresses introduced into the specimen by severe plastic deformation. Another alternative is that nucleation of the β'' phase starts already at 80°C. Positron trapping at new defects introduced by the nucleation of the β'' phase prevents the decrease of I_2 even when the dislocation density decreases. The abrupt drop in HV is reversed at 100°C by a slight increase caused by formation of fine precipitates of the β'' phase which cause a weak precipitation hardening. At the same time recovery of dislocations continues which is confirmed by a strong decrease in I_2. Thus, in the temperature range 100–220°C two competitive processes take place in the HPT-deformed Mg9Gd specimen: (i) precipitation hardening and (ii) softening caused by recovery of dislocations. Fig. 6A shows TEM image of HPT-deformed Mg9Gd specimen annealed up to 160°C. No precipitates could be recognized in bright-field TEM images due to still a high density of dislocations and also due to very small size of β'' phase particles. Recovery of dislocations inside grains is well visible in Fig. 6B showing the specimen annealed up to 220°C.

At higher temperatures the metastable β'' phase dissolves and particles of the stable β phase are formed. The β phase precipitates were identified by TEM in the specimen annealed up to 260°C. Finely dispersed incoherent particles of the β phase cause higher hardening which is reflected by a local maximum of HV at 250°C, see Fig. 5A. Further growth of the β phase precipitates leads again to a decrease of HV above 250°C A bright-field TEM image of HPT-deformed Mg9Gd specimen annealed at 300°C is shown in Fig. 7. A significant decrease in the dislocation density can be clearly seen. However, the grain size does not increase and remains at about 100 nm demonstrating very good thermal stability of the UFG structure in this alloy. Hence, recovery of dislocations in HPT-deformed Mg9Gd is not accompanied by grain growth. This is likely due to fine β phase precipitates which inhibit migration of grain boundaries and efficiently prevents grain growth. For comparison HPT-deformed pure Mg is fully recrystallized already at 200°C [14]. The local maximum in I_2 at 300°C reflects precipitation of the equilibrium β phase. It is in concordance with the HV curve. Positrons are trapped at the misfit defects between the incoherent β phase particles and the matrix. This results in a local increase in I_2. Coarsening of the β phase particles causes a subsequent decrease in I_2, see Fig. 5B. Bright-field TEM images of HPT-deformed Mg9Gd specimen annealed up to 380°C are shown in Fig. 8. These figures clearly demonstrate that annealing above 300°C leads to a noticeable grain growth, which causes an increase of the mean grain size up to a few microns. Above 450°C, the β phase particles dissolve and the solid solution is restored.

From our investigations we can conclude that the precipitation sequence in HPT-deformed Mg9Gd differs significantly from that known in corresponding coarse-grained material. Contrary to the coarse-grained solution treated alloy, precipitation of the stable β phase is shifted to significantly lower temperatures. Moreover, the β phase precipitates in HPT-deformed alloy are definitely finer that precipitates of this phase in solution treated specimens. This is demonstrated by the fact that contribution of positrons trapped at misfit defects at the interfaces of β phase particles is below the sensitivity threshold of LT measurements in the solution treated alloy, while in the HPT-deformed specimen this contribution was clearly identified as a distinct peak centered at 300°C in the temperature dependence of I_2, see Fig. 5B. Density of the fine β phase particles in HPT-deformed specimen is higher than density of coarser β particles in solution treated alloy. This leads to a higher contribution of positrons trapped at misfit defects at the interfaces of the fine β phase particles. Finally it has to be mentioned that existence of the fine β phase particles, which efficiently inhibit grain growth, explains the enhanced thermal stability of UFG structure in HPT-deformed Mg9Gd alloy.

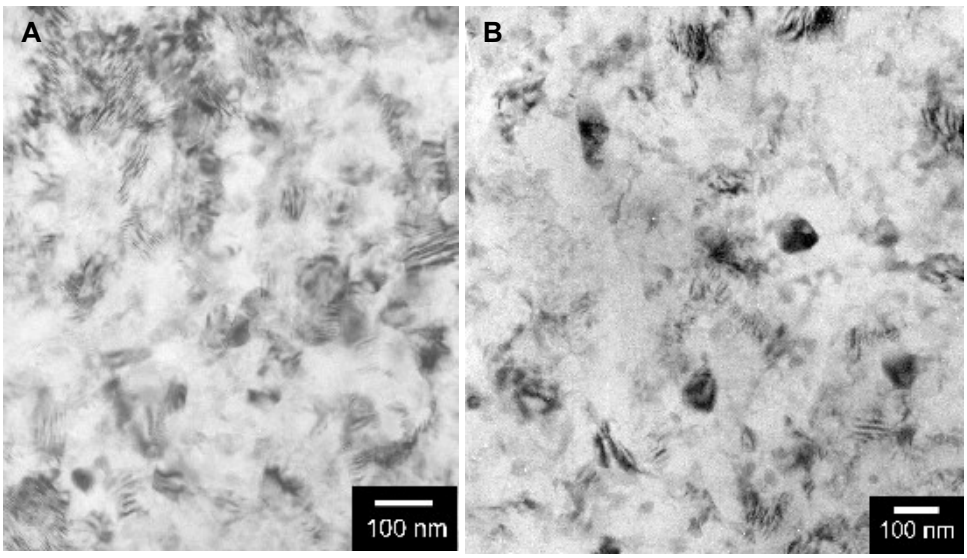

Fig. 6 Bright-field TEM image of HPT-deformed Mg9Gd alloy annealed up to: (A) 160°C (B) 220°C.

Contrary to the solution treated alloy, the metastable β' phase was not clearly recognized in the HPT-deformed Mg9Gd specimen. Hence, either this phase is absent in HPT-deformed alloy and β'' phase is replaced directly by the stable β phase, or it is formed, but in such case its formation is shifted to lower temperatures in similar way as β phase. Temperature range where β' could be probably formed is indicated in Fig. 5, but since it was not undoubtedly identified it is denoted with a question mark.

Thus, precipitation of β phase and probably also formation of β' phase start at significantly lower temperatures in HPT-deformed alloy. It has two reasons: (i) extremely small grain size leads to a significant volume fraction of grain boundaries. Defects at grain boundaries serve as nucleation centers for the second phase particles. (ii) Self-diffusion and diffusion of Gd atoms is enhanced by a possibility to diffuse along grain boundaries. Both these factors facilitate precipitation effects in the UFG alloy and shift phase transitions to lower temperatures.

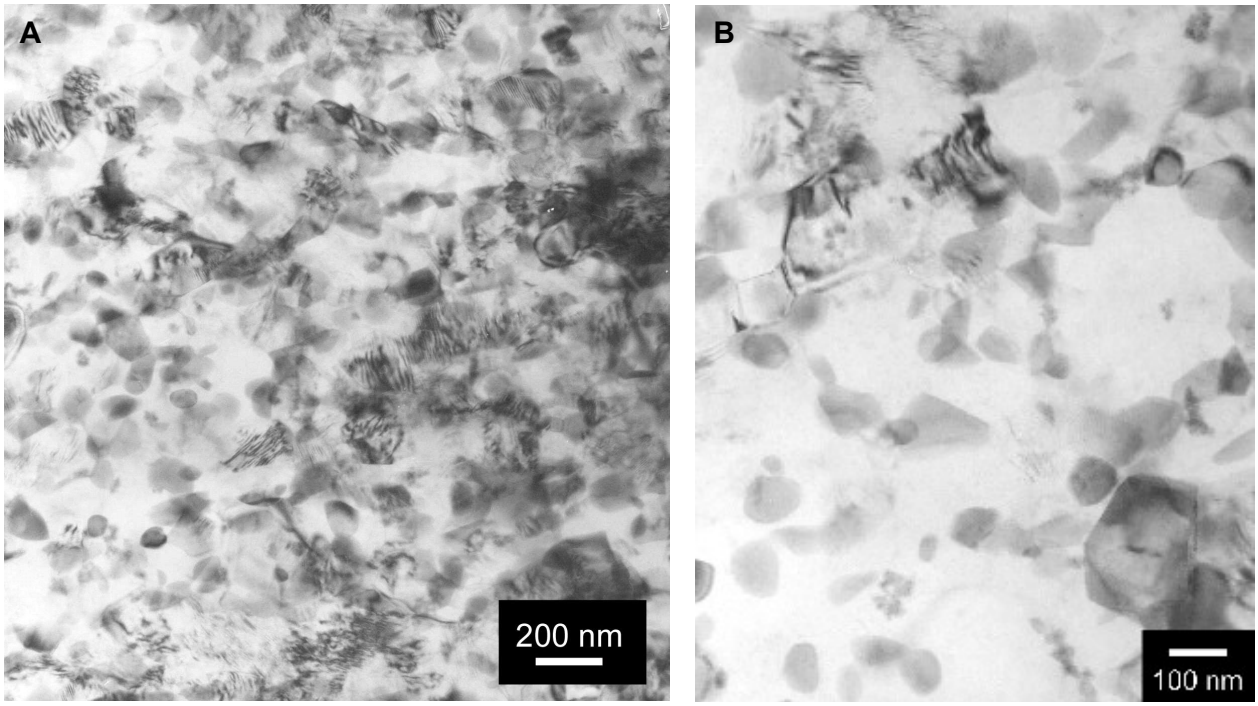

Fig. 7 Bright-field TEM images of HPT-deformed Mg9Gd alloy annealed up to 300°C.

Ductility of HPT-deformed alloy. High thermal stability of UFG structure in HPT-deformed Mg9Gd alloy is favorable for ductility. Fine grains persisting up to elevated temperatures due to the stabilizing effect of fine precipitates enable e.g. grain boundary sliding during plastic deformation, and should have, thereby, a positive impact on ductility of HPT-deformed alloy. In order to examine ductility of HPT-deformed specimen and compare it with the conventional solution treated alloy, we performed deformation tensile tests with constant strain rate. The stress-strain curves measured on HPT-deformed Mg9Gd specimen subjected to tensile tests at 400°C using three different strain rates are plotted in Fig. 9A. The actual specimens prior and after the tensile test are shown in Fig. 9B. One can see that the peak flow stress strongly increases with increasing strain rate and at higher strain rates the hardening stage is followed by a region with negative slope in the stress-strain curve, which is typical for dynamical recovery. Note that similar shape of the stress-strain curves were recently measured on HPT-deformed Ni_3Al intermetallic [15]. The maximum elongation to failure of HPT-deformed Mg9Gd specimen in all tensile tests exceeded 250 % and for slower strain rates ($< 10^{-2}$ s^{-1}) it exceeded even 450 %. No macroscopic necking could be observed on the strained specimens. Hence, HPT-deformed Mg9Gd alloy exhibits a super-plastic behavior at 400°C. This is a

huge improvement of ductility compared to solution treated Mg9Gd alloy, which in tensile test performed at 400°C with the strain rate of 4×10^{-4} s^{-1} exhibited maximum elongation to failure of 70% only.

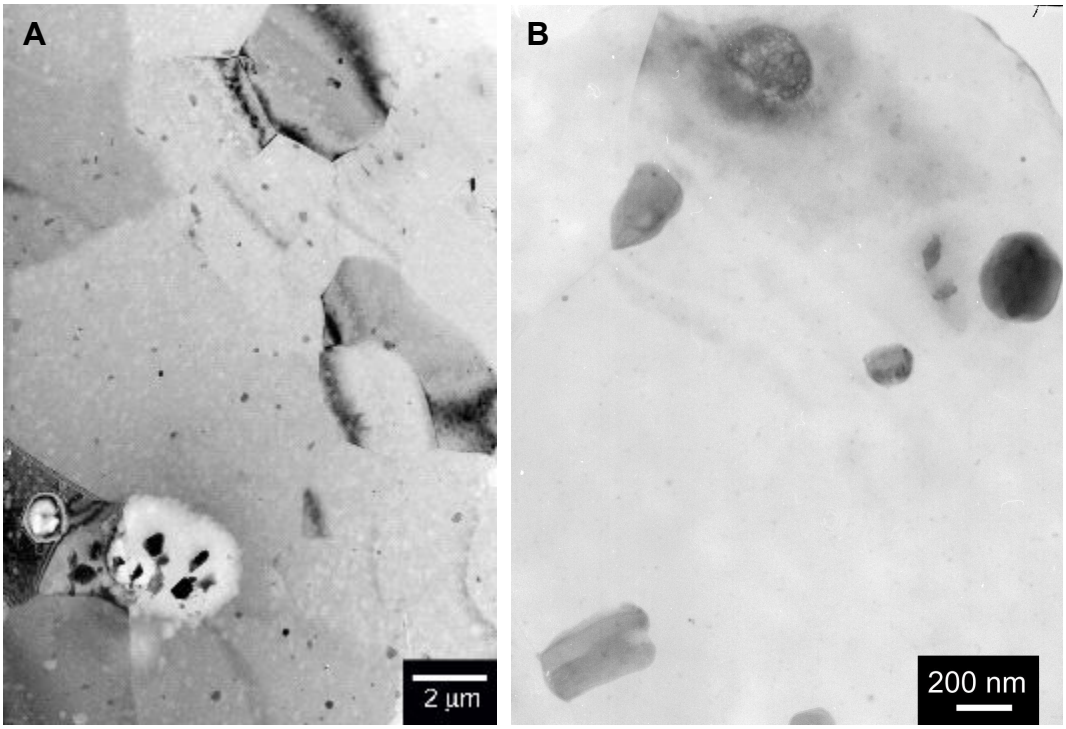

Fig. 8 Bright-field TEM images of HPT-deformed Mg9Gd alloy annealed up to 380°C.

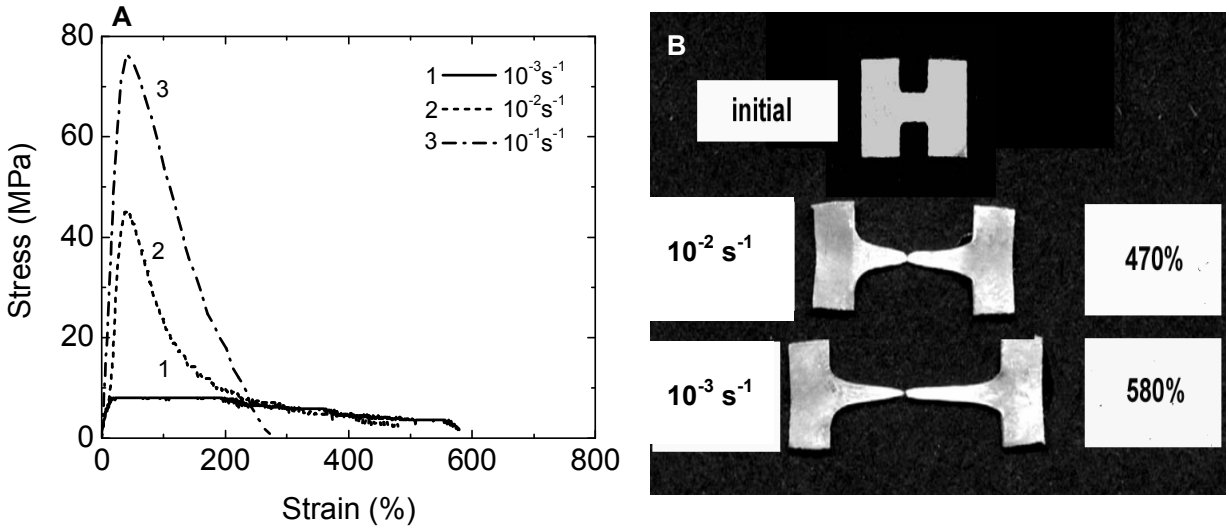

Fig. 9 Results of tensile tests of HPT-deformed Mg9Gd alloy: (A) stress-strain curves for strain rates 10^{-1} s^{-1}, 10^{-2} s^{-1}, and 10^{-3} s^{-1}, (B) actual specimens of HPT-deformed Mg9Gd alloy prior and after tensile tests with strain rates 10^{-2} s^{-1} and 10^{-3} s^{-1}. All tensile tests were performed at 400°C.

Summary

HPT-deformed Mg9Gd alloy exhibits a grain size around 100 nm and a high density of homogeneously distributed dislocations. An extreme grain size reduction and increase of dislocation density lead to a significant rise of hardness of the HPT-deformed alloy. Temperature development of microstructure of the HPT-deformed alloy was studied and compared with the coarse grained

sample. Recovery of dislocations in HPT-deformed alloy takes place in the temperature interval (100-220)^{o}C, but is not accompanied by grain growth. The mean grain size remains at around 100 nm up to 300^{o}C demonstrating very good thermal stability of UFG structure due to fine precipitates which prevent grain growth. Decomposition sequence in the alloy with UFG structure differs from that in the coarse grained solution treated alloy. Namely the precipitation of the β phase starts at remarkably lower temperatures and β phase particles are significantly finer than in solution treated alloy. It was found that HPT-deformed Mg9Gd alloy exhibits superplastic behavior at 400^{o}C. Ductility of HPT-deformed alloy was significantly enhanced compared to solution treated alloy due to fine grains persisting up to elevated temperatures.

Acknowledgements

Financial support from The Ministry of Education, Youth and Sports of The Czech Republic (project No. MS 0021620834) and The Academy of Science of Czech Republic (projects KAN300100801) is highly acknowledged.

References

[1] B.L. Mordike, Mat. Sci. Eng. A Vol. 324 (2002), p. 103.

[2] T. B Massalski, *Binary Alloy Phase Diagrams*, Vol. 3 (ASM International, Materials Park OH, 1990).

[3] P. Vostry, B. Smola, I. Stulikova, F. von Buch, B.L. Mordike, phys. stat. sol. (a) Vol. 175 (1999), p. 491.

[4] J. Cizek, I. Prochazka, B. Smola, I. Stulikova, R. Kuzel, Z. Matej, V. Cherkaska, phys. stat. sol. (a) Vol. 203 (2006), p. 466.

[5] R.Z. Valiev, R.K. Islamgaliev, I.V., Alexandrov, Prog. Mat. Sci. Vol. 45 (2000), p. 103.

[6] P. Hautojärvi, C. Corbel, in: *Proceedings of the International School of Physics "Enrico Fermi"*, edited by A. Dupasquier, A.P. Mills, Course CXXV, IOS Press, Varena (1995), p. 491.

[7] F. Becvar, J. Cizek, L. Lestak, I. Novotny, I. Prochazka, F. Sebesta, Nucl. Instr. Meth. A Vol. 443 (2000), p. 557.

[8] R.S. Mishra, R.Z. Valiev, S.X. McFadden, R.K. Islamgaliev, A.K. Mukherjee, Philos. Mag. A Vol 81 (2001), p. 37.

[9] R. N. West, in: *Positrons in Solids,* Topics in Current Physics Vol. 12, edited by P. Hautojärvi, Springer, Heidelberg (1979), p. 88.

[10] P. Tzanetakis, J. Hillairet, G. Revel, phys. stat. sol. (b) Vol. 75 (1976), p. 433.

[11] J. Cizek, I. Prochazka, B. Smola, I. Stulikova, R. Kuzel, Z. Matej, V. Cherkaska, R.K. Islamgaliev, O. Kulyasova, Mater. Sci. Forum Vol. 482 (2005), p. 183.

[12] J. Cizek, O. Melikhova, I. Prochazka, J. Kuriplach, I. Stulikova, P. Vostry, J. Faltus, Phys. Rev. B Vol. 71 (2005) 064106.

[13] J. Cizek, I. Prochazka, B. Smola, I. Stulikova, R. Kuzel, Z. Matej, V. Cherkaska, R.K. Islamgaliev, O. Kulyasova, Acta Phys. Polym. A Vol. 107 (2005), p. 738.

[14] J. Cizek, I. Prochazka, B. Smola, I. Stulikova, R. Kuzel, Z. Matej, V. Cherkaska, R.K. Islamgaliev, O. Kulyasova, Mat. Sci. Eng. A Vol. 462 (2007), p. 121.

[15] R.Z. Valiev, R.K. Islamgaliev, I.P. Semenova, Matr. Sci. Eng. A Vol. 463 (2007), p. 2.